frontiers in Energy Research

ORIGINAL RESEARCH
published: 14 October 2020
doi: 10.3389/fenrg.2020.00177

Experimental Determination on Shale Gas Loss During the Coring Process in Eastern Sichuan Basin

Junbo He[1,2], Jiren Tang[1,2]*, Jing Zhang[1,2], Yuanfei Ling[1,2] and Dongxu Jin[3]*

[1] State Key Laboratory of Coal Mine Disaster Dynamics and Control, Chongqing University, Chongqing, China, [2] National and Local of Gas Drainage in Complex Coal Seam, Chongqing University, Chongqing, China, [3] CNPC Chuanqing Drilling International Petroleum Engineering Co., Ltd., Chengdu, China

Shale gas loss by leakage directly affects the accurate measurement of shale gas content during drilling and coring. To accurately calculate shale gas loss, in combination with the actual situation of the shale coring, considering the influence factors of the main occurrence state of shale gas (free state and adsorption state), by means of treating the three stages of the shale well core removal, ground exposure, and water bath heating and desorption as a process of desorption that changes with confining pressure, an indoor shale gas loss simulation experiment method was independently designed to determine shale gas loss. Two sets of samples with large differences in physical properties in eastern Sichuan were selected for the shale gas loss simulation experiment. We proposed to use the error reduction rate of shale gas loss (the percentage of the difference between the shale gas loss obtained by the simulation experiment method and the rate obtained by the improved USBM method and curve fitting method and the amount of gas loss of core injected) to verify the accuracy of the simulation experiment method. The results show that compared with the improved USBM method, the average error reduction rate of cores by the experiment method were: 8.64%. Compared with the curve fitting method, the average error reduction rate of cores by the experiment method were 25.11%, which proved that the shale gas loss simulation experiment method had higher accuracy.

Keywords: shale gas, shale gas loss, calculation method, error reduction rate, coring

OPEN ACCESS

Edited by:
Bamidele Victor Ayodele, Universiti Tenaga Nasional, Malaysia

Reviewed by:
C. K. Cheng, Universiti Malaysia Pahang, Malaysia
Fahim Fayaz, Jawzjan University, Afghanistan

****Correspondence:***
Junbo He
627968213@qq.com
Jiren Tang
jrtang2010@163.com;
1806146981@qq.com

Specialty section:
This article was submitted to Advanced Fossil Fuel Technologies, a section of the journal Frontiers in Energy Research

Received: *09 May 2020*
Accepted: *08 July 2020*
Published: *14 October 2020*

Citation:
He J, Tang J, Zhang J, Ling Y and Jin D (2020) Experimental Determination on Shale Gas Loss During the Coring Process in Eastern Sichuan Basin. Front. Energy Res. 8:177. doi: 10.3389/fenrg.2020.00177

INTRODUCTION

In recent years, shale gas has become a hot spot in energy research around the world because of its huge reserves and as it creates less pollution in the environment (Li et al., 2014). The resource quantity of gas in shales is a prerequisite for the efficient exploration and development of shale gas. True determination of the gas content in shale at a representative location is a necessary condition for exactly determining the resource amount of gas in shales. During the coring process of shale gas wells, shale gas content mainly includes shale gas loss, desorption gas, and residual gas (Su et al., 2017). The quantity of shale gas loss directly affects the determination of shale gas content, and has a very important role in the exact evaluation of the resource quantity of gas in shales (Dong et al., 2012).

To exactly calculate shale gas loss during the coring process, domestic and foreign experts have conducted a great deal of research. At present, the main calculation methods include: the improved USBM method, the Smith-Williams method, the curve fitting method, and the indirect test method (Liu et al., 2010; Hao et al., 2015; Wei et al., 2015). The improved USBM method is based on the USBM (the US Bureau of Mines) method which estimates shale gas loss. In the initial stage of coring, according to the linear relationship between the sample desorption amount and the square root of desorption time, shale gas loss is obtained. However, the time of shale coring is relatively longer, and cracks unevenly develop, resulting in a large deviation of the shale gas loss (Yao et al., 2016; Wei et al., 2018). The assumption used in the Smith–Williams method is a single-porosity model. From the time of drilling to the time when the core is returned to the ground, the mud pressure changes linearly with time, and the solution of the single-porosity diffusion model is obtained (Smith and Williams, 1984). The curve fitting method is established by the solution fitting of all desorption data and the diffusion equation by Yee et al. (1993). According to the desorption amount of shale gas and desorption time data obtained from the shale coring site, the relationship between the shale desorption amount and desorption time is fitted, and shale gas loss in the coring phase is then derived. However, a rock sample in a desorption tank in the field cannot be immediately balanced to the reservoir temperature in the water bath, and the desorption data measured when the core is lifted to the ground cannot correctly reflect the desorption law (Meng et al., 2013; Yang et al., 2016). In addition, the curve fitting method uses the inversion method to obtain the shale gas loss with desorption data after several hours, which must lead to a large error (Su et al., 2017). Seidle and Metcalfe (1991) fitted all the desorption data into the diffusion equation which gives the best estimates of lost gas. Wang et al. (2016) found that when the drilling depth was large, as the depth of the well increased, the estimation error of the loss became larger and larger. The estimating volume of lost gas in shale by these three methods will underestimate the gas content of the reservoir. Combined with the known measured desorption gas and residual gas, the indirect method can also be used to obtain the amount of shale gas loss. For example, the results of the isothermal adsorption test reflected the shale's ability to adsorb methane gas, which is used to evaluate the amount of shale adsorbed gas and determine the level of gas saturation. The logging interpretation method can use the reservoir porosity and gas saturation to calculate the free gas content, but the accuracy of many of these parameters and the residual gas are worth further study.

Scholars from around the world have carried out a series of gas loss simulation experiments for gas loss. Shang et al. carried out the calculation of leakage loss by reducing free gas in a tank or filling with water and recording intermittent readings (Shang, 2014). Kong and Song (2012) analyzed the CBM content testing technology and influencing factors and pointed out that according to national standards, there is a large error when testing coalbed methane content. Xu et al. simulated the loss of coalbed methane in the process of rope coring through laboratory experiments, using helium gas calibration of free space volume, a temperature control system, and a more accurate measurement system, providing a basis for evaluating the loss of gas obtained from various mathematical models (Xu, 2005). Yang et al. (2010) conducted physical simulation tests to determine the amount of coalbed methane emissions under drilling fluid conditions. Vacuum control, temperature control, charge compensation, and pressure drop linear control were used, but the effects of freedom were not considered. Zhang (2009) carried out a simulation test to determine gas loss during the process of drilling and coring. The distinctive feature of that study was that high-pressure water was used to discharge free space based on previous work. The desorption rules of methane gas in three consecutive stages of simulated core drilling, ground exposure, and containment in a sealed tank were revealed. However, shale gas and coal bed gas have very different core extraction times, proportions of adsorbed gas, and gas content. Therefore, based on the advantages and disadvantages of the above methods, it is necessary to explore new shale gas loss calculation methods.

In order to establish a shale loss gas calculation method with higher preciseness, according to the characteristics that shale gas mainly exists in free and adsorbed states, and the coring time is relatively long, drawing on the principle that the shale gas loss increases as the confining pressure decreases during the experimental measurement of gas loss in coal seam, an experimental method for shale gas loss is proposed. Drawing on the advantages and disadvantages of domestic and foreign scholars in designing simulation methods for gas loss in coal seams, combined with the characteristics of shale gas, an indoor shale gas loss simulation experiment platform is established. It can directly measure shale gas loss of samples during the coring process. Compared with the improved USBM method, it is not necessary to satisfy the linear relationship between the amount of desorption and the square root of desorption time at the initial stage of desorption. This platform also avoided the issue that the fitting methods used the core desorption data after several hours to invert the cumulative desorption amount before several hours. It has a wide range of application prospects.

EXPERIMENTAL PROCEDURE

Shale Specimens

Sample Description

The shale specimens were collected from the Silurian Long Ma Xi formation and the lower Cambrian Niutitang formation, which is the most successful shale-gas-producing area in China (**Figure 1**). A series of shale sample characterization analyses were conducted to determine the basic parameters including the total organic carbon content (TOC), the vitrinite reflectance (R_0) and mineral compositions. The geochemical data and the mineral compositions of the shale sample is shown in **Tables 1–3**. The average TOC and R_0 of the shale sample are 3.96 and 2.59%, respectively, which are of the optimal range for the occurrence of shale gas (TOC > 2%, 3% > R0 > 1%) (Zhang et al., 2011). In this area, the source of the cored rocks are mainly composed of carbonaceous shale, siliceous

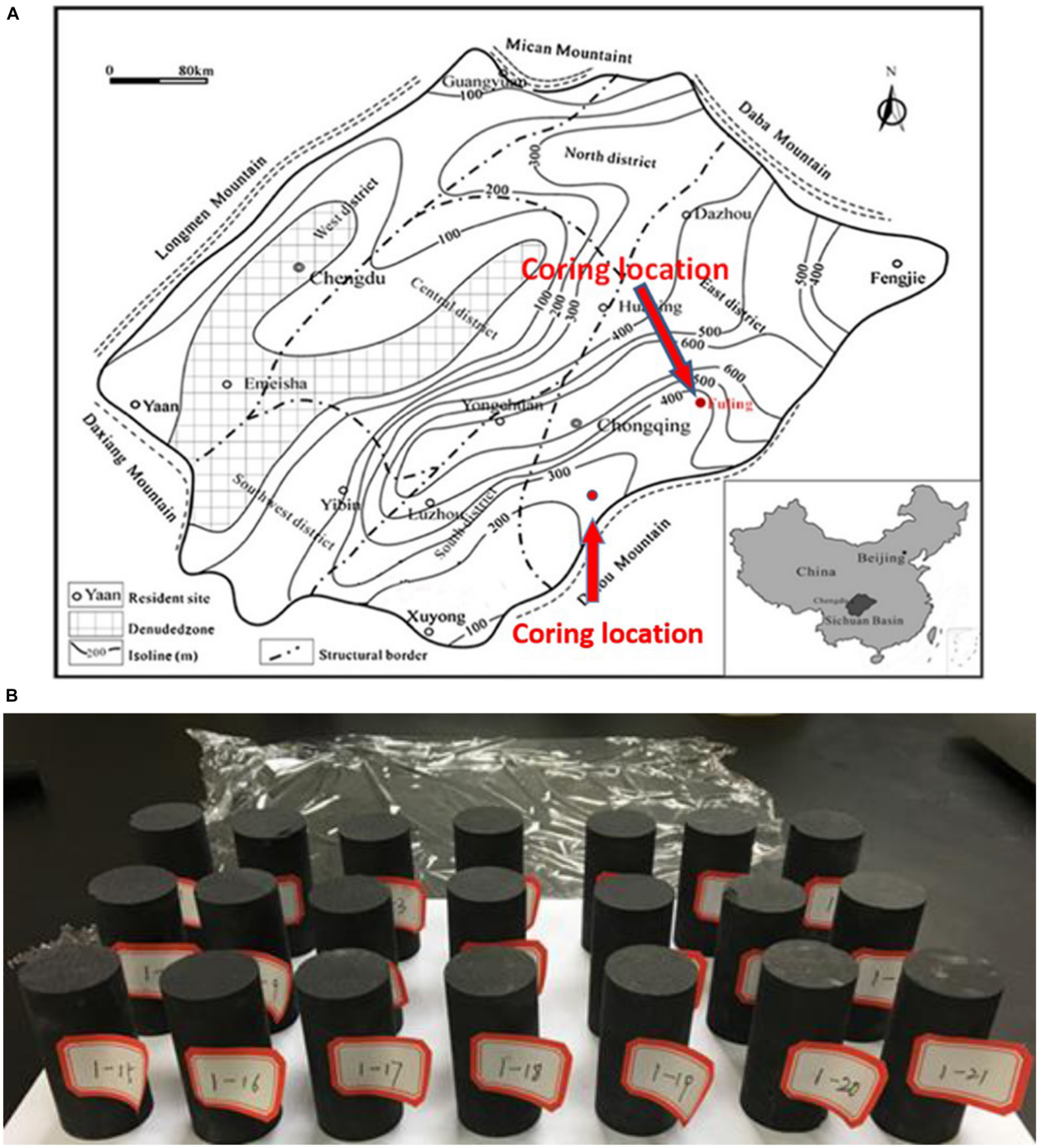

FIGURE 1 | (A) Location (insert) and topographic maps showing the shale drilling site. **(B)** Shale specimens before they were broken.

shale, silty shale, and lime-rich shale (Ray et al., 2010; Tinni et al., 2018). Four sets of representative samples with different depths of target layers were collected from the Silurian Longmaxi formation (core 1146, core 1162) and the lower Cambrian Niutitang formation (core 1427, core 588) from FY well and YC well in eastern Sichuan basin, and the gas production in the FY well was better than that of the YC well. According to SY/T 6940-2013[1], the measurements of sample quality, sample volume, and site-based coring parameters such as saturation pressure and reservoir temperature are provided in **Tables 1–3**. According to GB/T 19559-2008[2], shale specimens were crushed

[1]SY/T 6940-2013, Shale gas content determination method.

[2]GB/T 19559-2008 Method for determination of CBM content.

TABLE 1 | Sample inflation compensation standard.

Sample	Depth (m)	Geological age	TOC	Pressure (MPa)	Temperature (K)
Core 1427	1,427	Niutitang formation	1.63	14.27	326.69
Core 588	588	Niutitang formation	2.53	5.88	309.91
Core 1146	1,146	Longmaxi formation	6.36	11.46	321.07
Core 1162	1,162	Longmaxi formation	5.31	12.13	322.41

TABLE 2 | Mineralogical composition (%) of shale samples.

Sample number	Quartz	Plagioclase	Calcite	Dolomite	Pyrite	Hematite	Clay	Potassium feldspar
Core1427	49.6	2.3	7	3.1	4.8	3.8	27.1	2.3
Core 588	51.5	2.2	7.1	3.5	4.7	–	26.1	2.2
Core 1146	51.4	1.4	4.9	2.5	3.8	–	31.9	1.4
Core 1162	44.3	1.9	5.6	2.7	4.8	–	35.5	1.9

TABLE 3 | Sample parameters.

Sample number	Specimen mass (g)	Specimen volume (ml)	Saturation pressure (Mpa)	Loss time (min)	$S_{g\%}$	Zs	Φ
Core 1427	285	120	14.27	190	11.5	0.8827	2.89
Core 588	355	150	5.88	65	5.6	0.9185	2.31
Core 1146	290	135	11.46	153	9.0	0.8841	3.44
Core 1162	285	125	12.13	162	6.6	0.8828	3.68

to approximately 1 cm particles and the samples were kept sealed in plastic bags.

Before the shale gas loss simulation experiment, a part of the samples were randomly selected for NMR testing to determine the porosity, gas saturation, and pore size distribution of the samples. Before carrying out NMR, it was necessary to conduct water saturation treatment on the shale specimens lasting 12 h in order to fill the pores with fluid containing H (water). Pore diameter distribution curves of the shale specimens are shown in **Figure 2**. Another part of the sample was made into

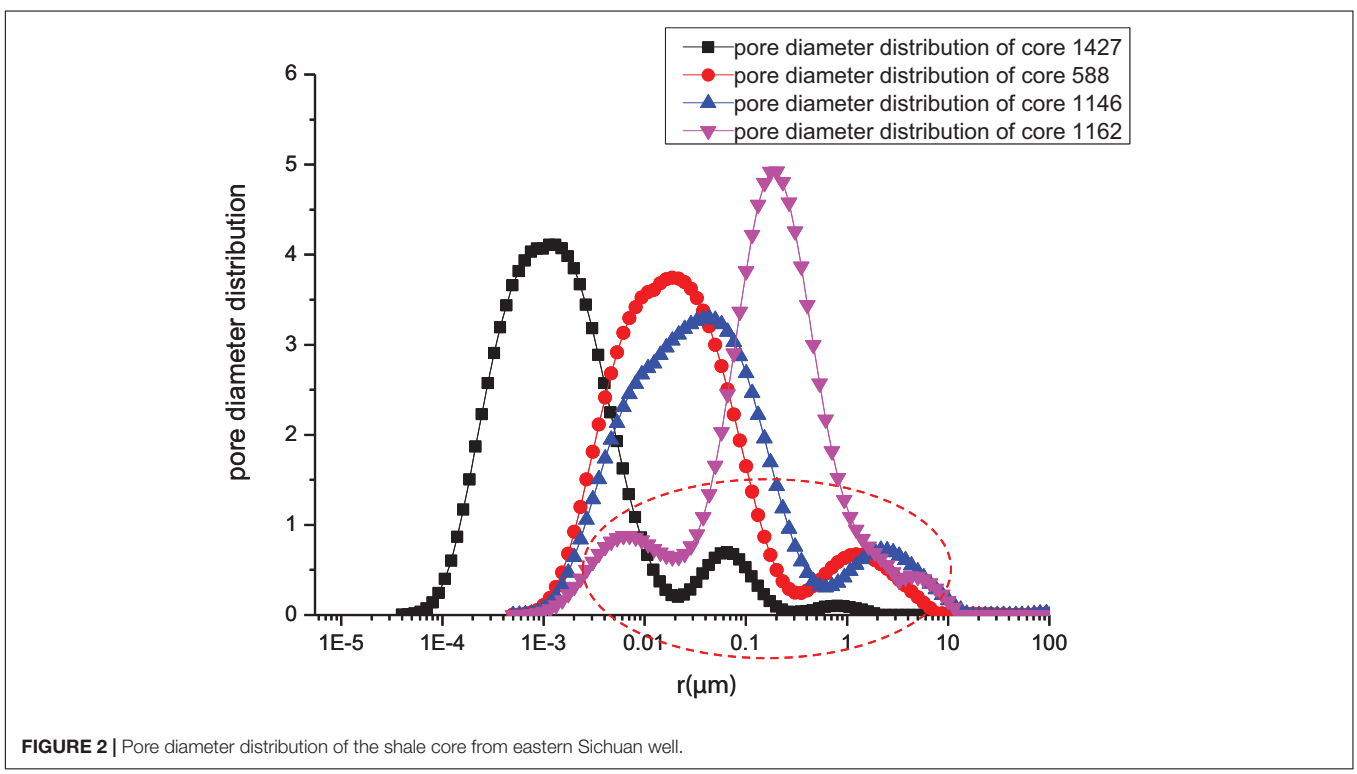

FIGURE 2 | Pore diameter distribution of the shale core from eastern Sichuan well.

250 micron particles, according to GB/T19560-2008[3], dried for methane isothermal adsorption tests to analyze the adsorption and desorption characteristics of samples under the conditions of heavy damage.

Simultaneously, part of this batch of shale specimens were dried at 110°C for 2 h, free water and adsorbed water were removed from the samples, and the samples were then vacuum-pumped for mercury intrusion tests. Another part of these samples about 10 g of the particles about 2 mm in size were first dried in a drying oven at 200°C for 8 h, and the ASAP2020 tests were then carried out to reveal the characteristics of the medium-microporous distribution, pore size, and the specific surface area of the samples.

Effects of Specimen Shape and Size

The equilibrium time for the inflation compensation of φ50 mm × 100 mm cylindrical specimens is difficult to determine. The reasons are that the shale is too dense, the shale texture is hard, micro-cracks develop, and the seepage resistance is high. It is difficult to have sufficient laboratory conditions to fully restore the samples to the reservoir state, especially too long after the coring time. The shale gas is mainly deposited in the interior of the rock body by physical adsorption, but there is still a very small amount in the form of chemical adsorption (Zhou et al., 2016). Therefore, there is a portion that has undergone irreversible chemisorption.

Thus, the cylindrical test piece was subjected to a certain degree of crushing. If the core of the wellbore has just been taken out, it can be directly cleaned and then inflated and restored to the original state of the reservoir. If the core of the wellbore has been taken out for several months, it can be crushed to about 1 cm, and after vacuuming, it can be tested according to the test procedure.

In this paper, the selection of shale particles with a particle size of about 1 cm instead of φ50 mm × 100 mm cylindrical specimens is based on the following assumptions:

(a) Compared with the almost infinite reservoir geologic body, the standard cylindrical shale test piece of φ50 mm × 100 mm and the irregular sample particle of about 1 cm particle diameter are equivalent samples. They are of the same order of magnitude relative to the shale gas reservoir.
(b) They have no large-scale destruction of the microstructure of the samples.
(c) The obtained law has similar field engineering guiding significance for the effective development of actual shale gas resources, and the influence on the microstructure of the specimen itself is within a certain error range.

Reversible Influence

In the reservoir, this state is caused by various geostress interactions over a long period of time. The shale gas represents the decomposition of kerogen in a large number of organic pores inside the test piece, and it is present in the micro-cracks and pores inside the reservoir in the free state and the adsorbed state.

Whether the decomposition of kerogen in organic pores is reversible, as well as whether it can restore its initial state by pressure change, raising the temperature of the specimen to the temperature of the reservoir, remains controversial, but the proportion of organic pores in the shale is small. The shale gas is decomposed from the organic matter, and the reservoir has a certain space. The fluid and total gas content in the reservoir are always in a relatively balanced state.

The whole process is complex and variable, including chemical adsorption, thermal decomposition, physical adsorption, as well as various factors such as biological and geological effects (Yee et al., 1993). However, the entire shale reservoir follows mass conservation, and the fluid in the pore micro-fractures is in equilibrium. When the confining pressure changes, the energy will slowly be conducted to the depth of the reservoir in the form of pressure waves, and the process is dominated by reversible physical changes and is in dynamic equilibrium or quasi-equilibrium. As the reservoir pressure decreases, the total gas volume adsorption/desorption and free gas release can be regarded as a physical reversible process.

Experimental Platform

According to the experimental test method of shale gas loss, when the core pressure was lower than the internal pressure of the core, the core began to desorb, and the amount of desorption increased with the increase in pressure difference during shale coring (**Figure 3**). An independently developed shale gas loss simulation experiment platform was used in the test (**Figures 4**, **5**). This device is composed of five parts: a constant-temperature water bath system; the main experimental system; a pressurization system; a data acquisition system; and desorption meter. Combining the known reservoir pressure, temperature, and calculated loss time of the sample, this experimental platform can accurately test shale gas loss during shale coring.

The precision of the constant-temperature water bath is 0.02°C, with a temperature range of 5–95°C. The heating pipe, temperature sensor, temperature regulator, and circulating pump are set in the constant-temperature water bath to guarantee uniformity of heating.

The main experiment system consists of a reference tank, adsorption tank, temperature sensor (PR-21 series, accuracy of 0.15°C, Omega, United States), pressure sensor (PX-409 series, Omega, United States; range 0–24.13 MPa, accuracy 0.03% of the full scale), piping, vacuum pump, and valves, with a system pressure of 24 MPa (**Figure 4**). The main experimental system is placed in the constant-temperature water bath, and experimental gas enters the adsorption tank after stabilization at constant temperature and pressure in the reference tank. The temperature sensor is placed in the reference tank, and the pressure sensor is connected to the reference tank by piping. The main functions of the main experimental system include: adsorption and desorption, vacuum, calibration of free space volume, and monitoring of pressure and temperature in the adsorption tank.

Two different pressurization systems were used. Methane gas was introduced by connecting a pressure-reducing valve to a methane gas cylinder at 15 MPa. Helium gas was introduced with a Teledyne ISCO 260D double plunger booster pump, which provided a maximum pressure of 51.7 MPa. The air

[3]GB/T 19560-2008, High-pressure isothermal adsorption test method for coal.

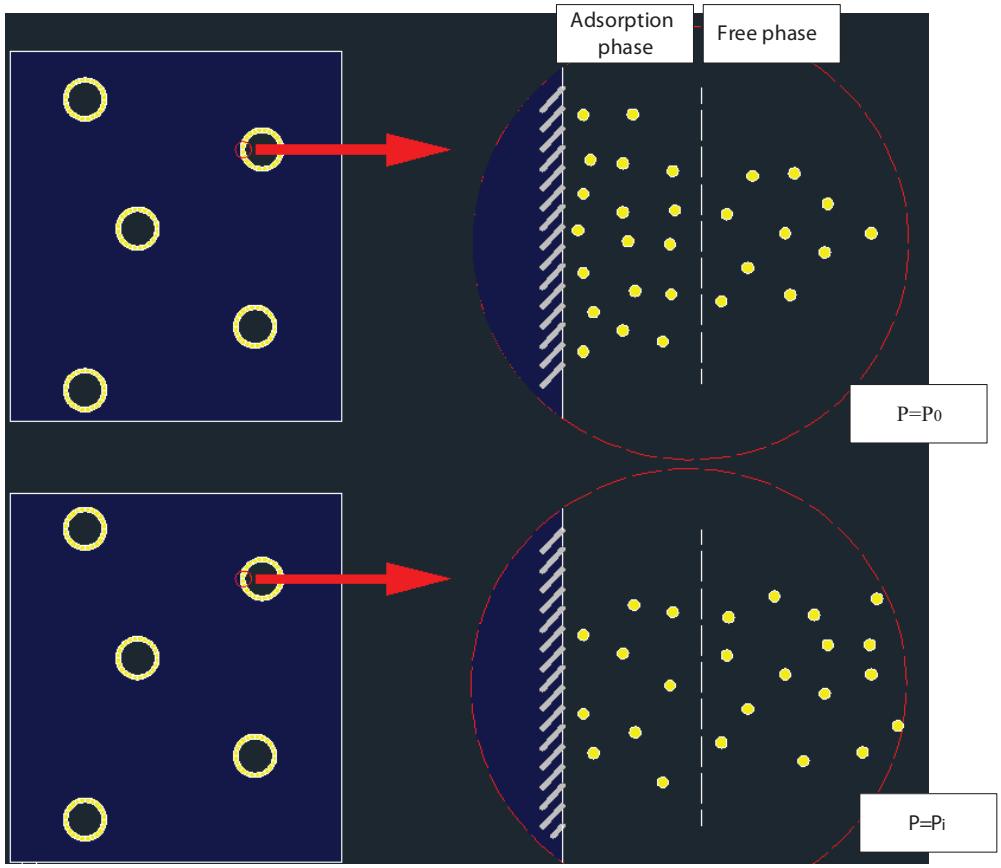

FIGURE 3 | Comparison of gas occurrence states of shale cores under different confining pressures.

inlet of the ISCO pump was connected to the helium cylinder, and the air outlet was connected to the reference tank through the pipe and valve.

The data acquisition system consists of a LabVIEW virtual instrument platform, a temperature sensor (PR-21 series, accuracy of 0.15°C, Omega, United States), and a pressure sensor (PX-409 series, Omega, United States; range 0–24.13 MPa, accuracy 0.03% of the full scale).

The desorber is mainly divided into a normal pressure desorber and a variable pressure desorber with a certain pressure drop gradient with an accuracy of 0.1 ml, and the two can be switched continuously.

The volumetric method was used to measure the amount of gas adsorbed in the sample following the method described in the literature (Sun et al., 2013). The contrast channel volume and volume of free space were calibrated with helium. REFPROP software was used to calculate the compression factors of helium and methane based on the gas state equation (Span and Wagner, 1996).

Error Analysis

Regarding the source of error, according to the previous analysis, the main source of systematic error is generated by the adsorption/desorption test process (Stotsky and Bortz, 2019). The relationships between the amount of adsorption and various factors are as Eq. 1.

$$n^{ex} = f\left(P, T, V_f, V_R, Z\right) \tag{1}$$

The free space volume is calculated from the reference slot volume. The compression factor Z is calculated from P and T, so the free space volume and the compression factor Z can be obtained from the above error recursion formula. The error quantities of the remaining measurement parameters are shown in **Table 4**.

According to the error transfer formula, the following can be obtained:

$$dn_i = \frac{dx_1}{x_1}x_1 + \frac{dx_2}{x_2}x_2 + \cdots + \frac{dx_n}{x_n}x_n \tag{2}$$

where dx_1/x_1 is the relative error β_i. Eq. 1 can be transformed into Eq. 3:

$$dn_i = \beta_1 x_1 + \beta_2 x_2 + \cdots + \beta_n x_n \tag{3}$$

In this paper, we can obtain$\beta_1 = 11.354\%$,$\beta_2 = 2.731\%$, $\beta_3 = 3.826\%$.

The variable β_1 is the error under high pressure; β_3 and β_2 are the error under low pressure. The above calculation results show that the error of the high pressure section is much

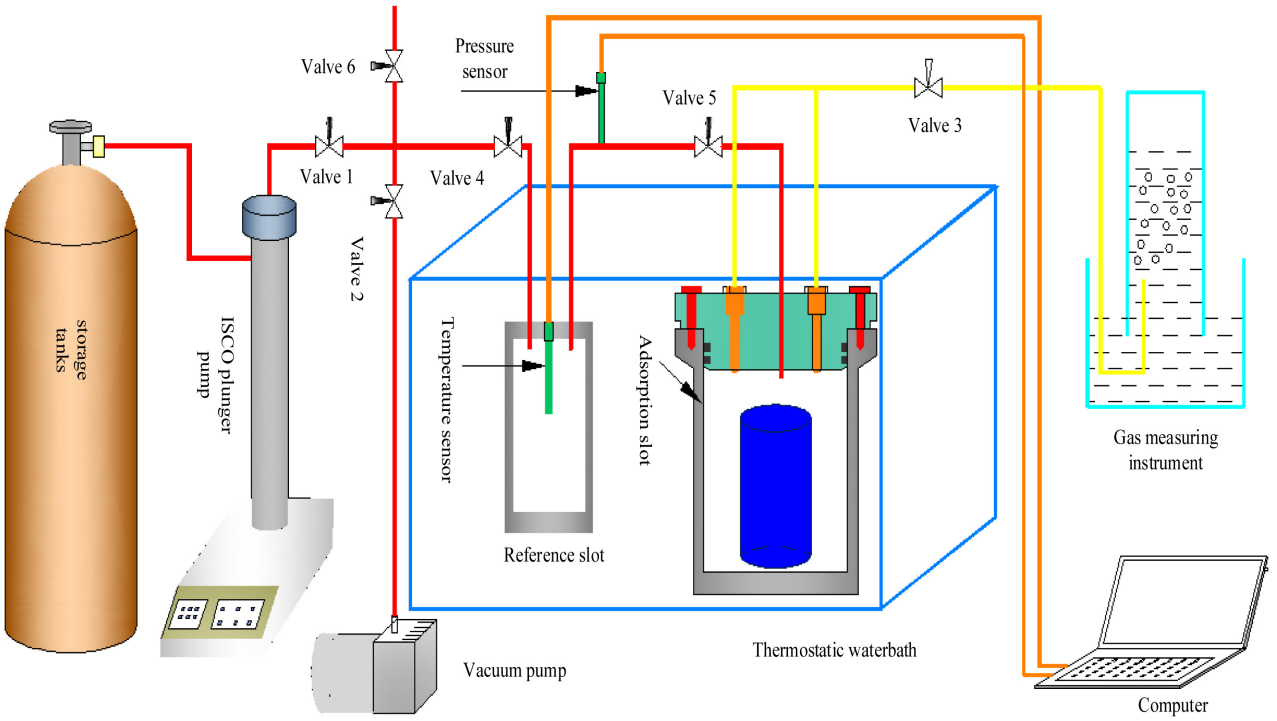

FIGURE 4 | Desorption-adsorption simulating testing device.

larger than that when the pressure is low when the volumetric method measures the adsorption amount, which results from the accumulation of errors in the volumetric measurement. At the same time, under the same conditions as in the other tests, a larger adsorption/desorption amount of the shale gas loss test system is associated with smaller experimental error. Therefore, the total adsorption/desorption amount can be increased by increasing the mass of the sample to reduce the experimental error.

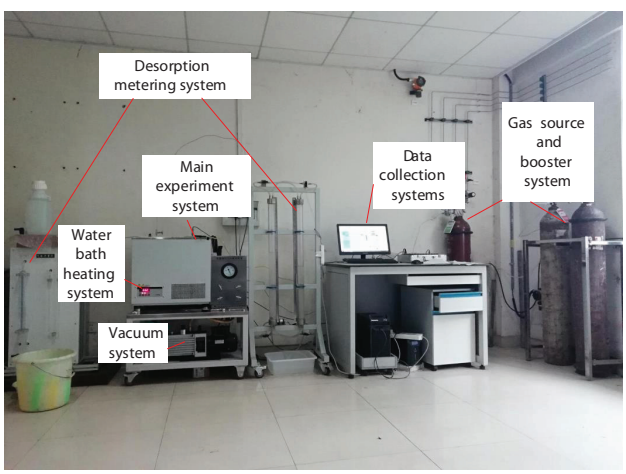

FIGURE 5 | Physical diagram of simulation experiment system of rock gas escape loss.

Experimental Method

Experimental Program

In addition to the shale gas loss simulation experiment, this study also includes some auxiliary experiments: firstly, a TOC test, Ro test, and XRD test were conducted to determine the basic parameters including the total organic carbon content (TOC), the vitrinite reflectance (R_0), and mineral compositions. Before the shale gas loss simulation experiment, most of the specimens were crushed to about 1 cm particles, while part of these samples about 10 g of particles about 2 mm size were used for methane isothermal adsorption testing and ASAP2020 testing. In addition, in order to obtain a more comprehensive microstructure to facilitate the comparative analysis of the accuracy of the shale gas loss simulation experiment method, mercury testing and NMR testing were also carried out. In the simulation experiment, the change of the saturation pressure and temperature have an impact on the mechanical properties of shale, so it was set to the saturation pressure and a constant temperature according to formation conditions. In theory, unlimited equilibrium time

TABLE 4 | The error of the amount of adsorption by any direct parameter measurement.

Parameter	Sensor	System error
P	omega Px409-3.5k-AL-XL	Accuracy: 0.03%
T	omega pr-21	±0.15℃
V_R	helium gas measurement	48.62 mL ± 2.45%

could frequently result in ultimate adsorption equilibrium between the CH4 and the shale. Under laboratory conditions, Tang et al. (2018) found that an equilibrium state of CO_2 adsorption on shales can be reached after 9–10 h. Therefore, the saturation time was set to 24 h to ensure that the specimens were saturated fully.

Experimental Steps

Due to shale gas containing 90% methane (Li, 2000), methane gas with 99.99% purity was used. The methane pressure was gradually increased from 0 to 15 MPa, with a total of seven test points, with an equilibrium time of at least 24 h for each test point. The steps in the experimental procedure were as follows.

(1) The processed samples were installed in the adsorption tank, and the pipes and data collection system were connected.
(2) A 24 h air tightness check of the whole system using helium gas was completed. The change in gas pressure in 24 h could not exceed 0.007 Mpa (pressure sensor accuracy).
(3) The constant-temperature water bath was heated to reservoir temperature and maintained to calibrate the free space volume in the sample tank.
(4) The vacuum pump was opened and the sample was vacuumed in the tank for 30 min.
(5) The charging gas was compensated into the core. Methane was injected, and the free space pressure under initial conditions was $P_{i-1}^{S,Eq}$; valve 1 and valve 4 were opened, valve 5 was closed, and the remaining valves were then closed (as shown in **Figure 4**). From the gas state equation, Eq. 4 can be concluded:

$$P_{i-1}^{S,Eq} V_F = Z_{i-1}^{S,Eq} n_{i-1}^{R,F} RT \tag{4}$$

The test gas was injected into the reference tank, valve 4 was then closed, and the pressure of the adsorption tank was finally stabilized to $P_i^{R,F}$ at the temperature T. From the gas state equation, Eq. 5 can be concluded:

$$P_i^{R,F} V_R = Z_i^{R,F} n_i^{R,F} RT5 \tag{5}$$

Then, valve 5 was opened, and gas was allowed to enter the adsorption tank. The pressure at the temperature T was finally stabilized to $P_i^{S,Eq}$. From the gas state equation, Eq. 6 can be concluded:

$$P_i^{S,Eq} (V_F + V_R) = Z_i^{S,Eq} n_i^{S,Eq} RT \tag{6}$$

The sample adsorption amount Δn_i^{ex} is as Eq. 7:

$$\Delta n_i^{ex} = \frac{1}{m} \left(n_{i-1}^{R,F} + n_i^{R,F} - n_i^{S,Eq} \right) \tag{7}$$

(6) Valve 5 and valve 3 were opened, and other valves were closed. Methane gas was allowed to enter the gas measuring instrument, as showed in **Figure 4**. The drilling fluid column pressure drop process around the shale core during drilling and core extraction was simulated. The pressure drop rate was controlled so that the pressure inside the tank dropped to atmospheric pressure during the loss time, and the gas discharge amount was measured.
As shown in **Figure 4**, valve 4 was closed to open valve 8, according to that the loss time of core 1427, core 588, core 1146, and core 1162 was 190, 65, 153, and 162 min (Su et al., 2017), respectively; and the formation condition of core 1427, core 588, core 1146, and core 1162 was 14.27 MPa, 55°C; 5.88 MPa, 37°C; 11.46 MPa, 48°C; and 11.62 MPa, 49°C, respectively. The pressure drop rate of the drilling liquid column around core 1427, core 588, core 1146, and core 1162 was 0.075 MPa/min; 0.090 MPa/min; 0.075 MPa/min; and 0.072 MPa/min. The gas discharge amount was measured with the drainage method.
(7) After the pressure was reduced to 0.1 MPa (atmospheric pressure), according to the shale gas content determination method SY/T 6940-2013 (see text footnote text 1), desorption measurement continued until the desorption end point. From these desorption data, the shale gas loss can be obtained by the linear fitting method and the curve fitting method.

In the experiment, the parameters such as pressure, temperature, time, and amount of gas discharged in the sample tank were recorded in detail by a microcomputer data acquisition system and the desorber, and atmospheric pressure and temperature values were simultaneously recorded. After this process was finished and the data were corrected, the characteristic curve of gas desorption in the sample over time can be obtained as well as the volume of shale gas loss during the simulation experiment.

Data Processing

Determination of Deviation Coefficient

The selection of an appropriate equation of state has an important influence on the calculation of the amount of adsorption/desorption. Many scholars have conducted extensive research on the state equation of methane from the perspective of thermodynamics. However, only a few models can accurately predict the density of methane in a wide range of temperatures and pressures. Among them, the SRK and RK equations of state which are widely used (Xiang et al., 2016).

According to the research results of Xiang et al., different gas state equations have different degrees of deviation from the phase description of methane, and the higher the pressure, the greater the deviation. In the shale isotherm adsorption experiment, the appropriate gas state equation must be optimized to calculate the amount of adsorbed gas and the amount of analytical gas. To calculate the phase change of the methane field, under low pressure (less than 10 MPa), the SRK equation should be used, and under high pressure (greater than 10 MPa), the RK equation should be used (Xiang et al., 2016).

Data Processing

The processing method of the test data is as follows. The gas volume discharged is as Eq. 8.

$$Q_{\mathrm{ei}} = \frac{V_d}{P_B} \times \left(\frac{P_0}{Z_0} - \frac{P_i}{Z_i}\right) \times \frac{T_B}{T_{i\mathrm{actural}}} \tag{8}$$

where, Q_{ei}—the gas volume discharged due to the pressure drop in the free space of the sample tank, ml;

V_d—free space volume of tank excluding sample, ml;
P_B—pressure in the standard gas state, MPa;
P_0—the initial pressure in the tank, MPa;
Z_0—when p is equal to P_0, CH_4 gas compression factor;
P_i—pressure in the tank, MPa;
Z_i —when p is equal to P_i, CH_4 gas compression factor;
T_B—standard state temperature, K;
$T_{iactural}$—in-tank actual temperature, K;

During the simulation test, when the pressure of the sample tank decreases, the gas volume discharged includes two parts. One part is the gas volume discharged due to the pressure drop in the free space of the sample tank (Q_{ei}), and the other part is the volume desorbed from the sample (Q_j). The volume of shale gas loss in sample is as Eq. 9.

$$Q_j = Q_i - Q_{ei} \tag{9}$$

where Q_j—the volume of shale gas loss in sample, ml;

Q_i—the total amount of gas discharged from the sample under different pressure differences, ml;

Q_{ei}—the gas volume discharged due to the pressure drop in the free space of the sample tank, ml.

RESULTS AND DISCUSSION

Results

Isothermal Adsorption Tests

The difference of bulk sample with a particle size of about 1 cm, powder with a particle size of 2 mm, and a standard cylindrical specimen ofφ50 mm × 100 mm at the same quality is that the degree of damage to the microstructure is different. For the same sample, the greater the degree of microstructural damage, the greater the adsorption/desorption and the shorter the time to reach equilibrium. According to **Figure 6**, after the samples have been crushed to 2 mm, isothermal adsorption experiments were performed at 30, 45, and 60°C. The max adsorption capacity of core 1427 and core 588 was 2.82 and 2.61 ml/g; The max adsorption capacity of core 1146 and core 1162 was 3.15 and 3.41 ml/g, which demonstrated that the same degree of microstructure damage was observed for the Silurian Longmaxi Formation and the lower Cambrian Niutitang Formation samples with significant differences in the physical properties selected in the experiments in this paper (both from φ50 mm × 100 mm cylindrical specimens to 2 mm). The adsorption capacity of Silurian Longmaxi samples was larger than that of the lower Cambrian Niutitang group. The adsorption/desorption of the Silurian Longmaxi Formation samples with better physical properties is still greater than that of the lower Cambrian Niutitang Formation samples.

Isothermal adsorption test results are helpful to explore the effect of the damage degree of the microstructure of the same sample on the adsorption capacity and adsorption equilibrium time. To reduce the influence of seepage resistance on the volume of the shale gas loss simulation experiment as much as possible, and to increase the feasibility of the experiment, the experimental sample was crushed from a φ50 mm × 100 mm cylindrical body to a particle with a diameter of about 1 cm. At the same time, it is considered that the purpose of the crushing is to prevent the shale gas from being injected only to the surface of the test piece due to the excessive resistance of the seepage. It is equivalent to establishing a high-speed channel for communicating micro-cracks in the deep part of the test piece.

Simulation Test Results

Equilibrium time

This paper adopts the relative particle hypothesis; that is, that the φ50 mm × 100 mm standard cylindrical shale test piece or the irregular particle sample with a particle size of about 1 cm is equivalent to an infinite shale reservoir geological body and the resulting law has similar field engineering guiding significance for the efficient development of actual shale gas resources.

In the adsorption tank, the 1 cm particle sample takes a relatively long time to inflate to reach equilibrium. During the sample gas injection process, the pressure in the sample tank continued to decrease with time, but the pressure drop rate gradually decreased. The conditions to reach equilibrium were that the pressure in the tank stabilized within a certain fluctuation range (0.007 MPa, pressure sensor accuracy). For the shale gas loss simulation experiment, after repeated tests, the corresponding equilibrium time was 24 h, as shown in **Figure 7**.

Injection amount

The injection amounts were determined based on the formation conditions of the shale cores. The formation condition of core 1427, core 588, core 1146, and core 1162 were 14.27 MPa, 55°C; 5.88 MPa, 37°C; 11.46 MPa, 48°C; and 11.62 MPa, 49°C, respectively. As shown in **Tables 1–3** and **Figure 8**, combined equilibrium time, the injection amount of core 1427, core 588, core 1146, and core 1162 were 2.72, 2.29, 2.86, and 3.19 ml/g, respectively. It showed that the sample injection amount of the Silurian Longmaxi Formation sample was higher than that of the lower Cambrian Niutitang Formation sample, which is consistent with the isothermal adsorption test results.

The desorption time

During the shale gas loss simulation experiment, when the pressure in the desorption tank began to decrease, it corresponded to the moment t_a when the field well core rises to the equilibrium point. Prior to this moment, it was the phase in which the gas did not escape. The time from the equilibrium point to the rise of the core to the ground is the shale gas loss escape phase (t_b) during pressure changes. Thereafter, the core pressure desorption stage is from the time the core is brought to the ground to the tank filling stage (t_c), followed by the time from the tank filling stage to the core desorption end stage (t_d).

$t < t_a$, the core does not escape the stage;
$t_a < t < t_b$, shale gas loss escape phase during pressure transformation;
$t_b < t < t_c$, shale gas loss escape phase at atmospheric pressure;

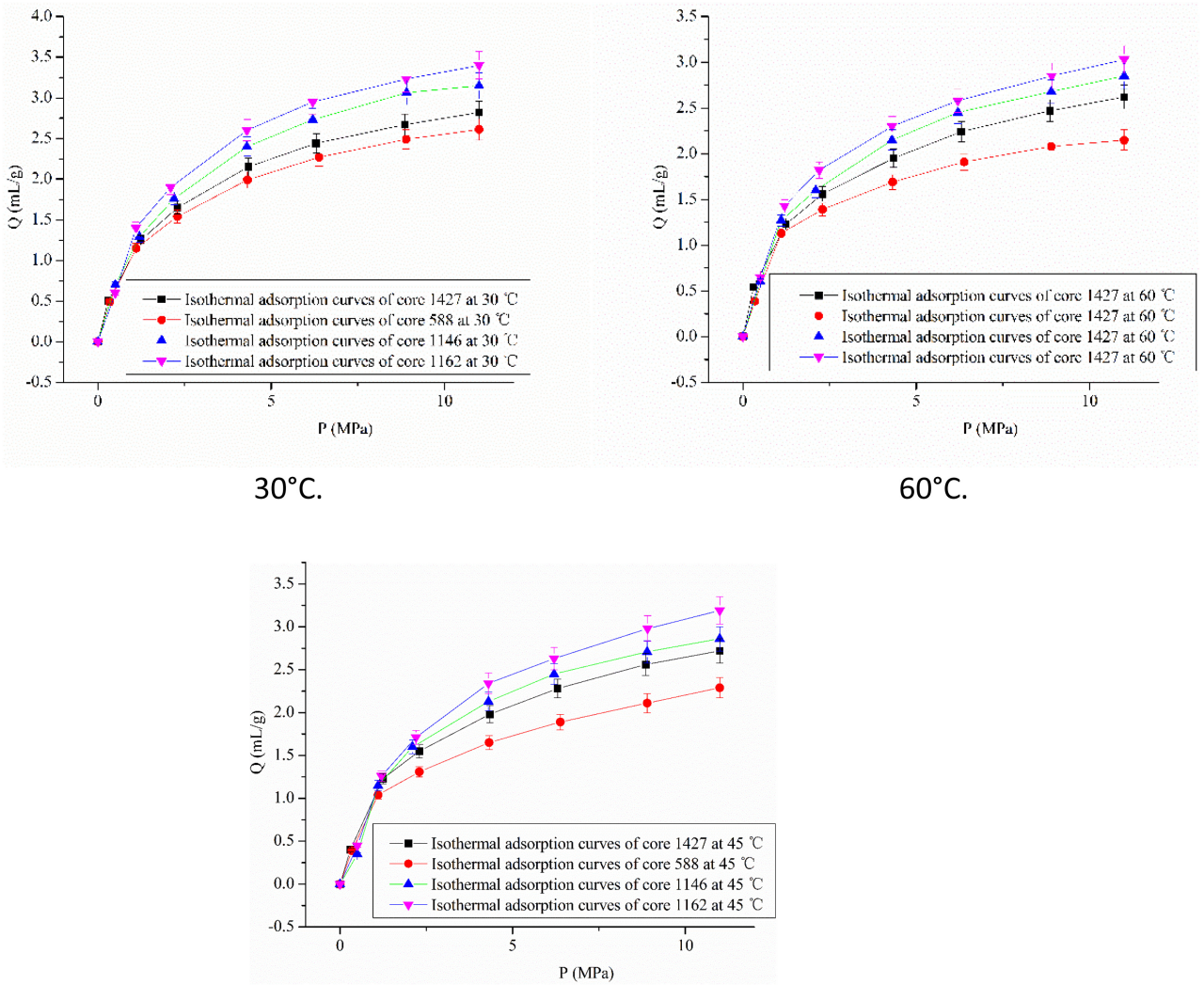

FIGURE 6 | Isothermal adsorption curve of samples at 30, 45, 60°C from eastern Sichuan well.

$t_c < t < t_d$, residual gas phase. The above is the different stages of shale gas dissipation during the entire shale coring process. The longer the t_b and t_c phases, the greater the amount of shale gas loss by escape. Controlling different pressure drop times, the gas loss simulation test data analysis shows that when there is no pressure change, the initial desorption amount has a linear relationship with the square root of desorption time. However, when the shale core is subjected to external pressure changes, the initial desorption amount is nonlinearly related to the square root of time.

Pressure and temperature

The balance and accurate measurement of the pressure of the entire system is very important. The effect of temperature on this process is obvious, which will inevitably affect the test results (Thommes et al., 2015). Therefore, the entire experimental process is particularly important for temperature control. When injecting gas, the temperature of core 1427, core 588, core 1146, and core 1162 were kept constant at 55, 37, 48, and 49°C, respectively. It slowly dropped to room temperature during the shale gas loss simulation experiment in shale after equilibrium.

During the coring process, according to the overall pressure change, it can be divided into three stages:

$P_{core} < P_{drillingfluidstring}$, the stage where shale gas loss does not occur;

$P_{core} = P_{drillingfluidcolumn}$, the moment when shale gas loss by escape begins;

$P_{core} > P_{drillingfluidcolumn}$, shale gas loss continues to occur with the pressure difference.

The curve of pressure with time when measuring the volume of shale gas loss was obtained in **Figure 9** and the relationship curve of the volume of shale gas loss over time in the experiment

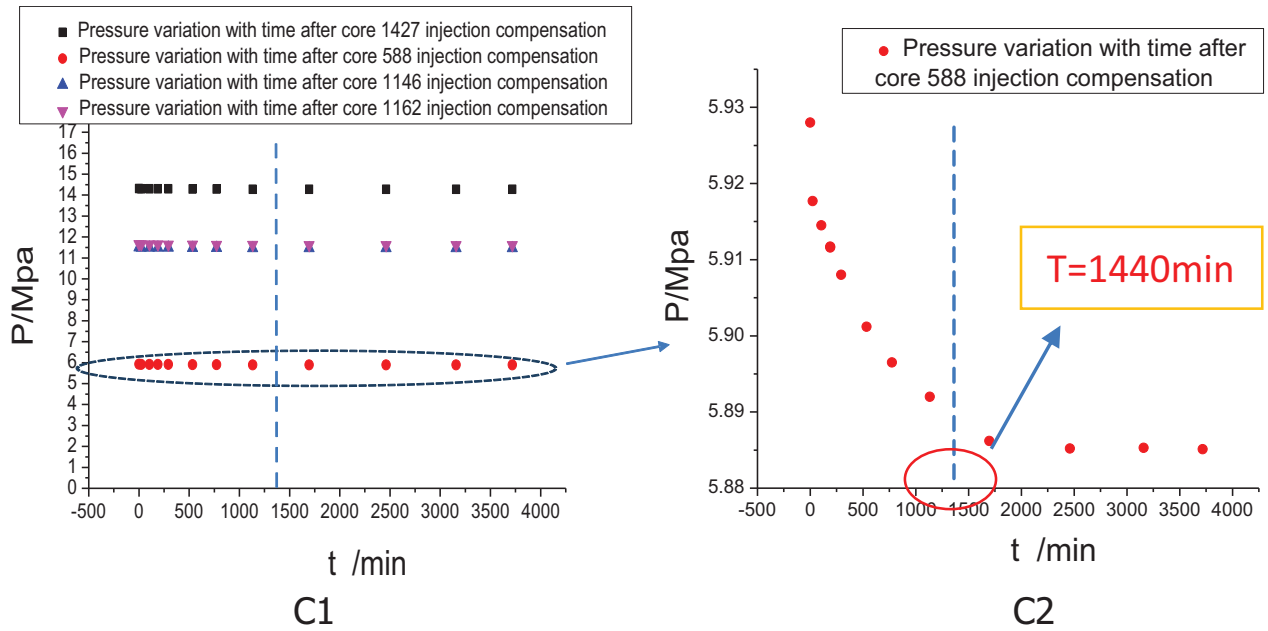

FIGURE 7 | The equilibrium time determination.

was acquired in **Figure 10**. Through the analysis of the shale gas loss simulation test data, it is concluded that:

a. In the early stage of desorption, the rate of desorption is small. When the confining pressure is gradually reduced, the pressure difference increases, desorption rate is also gradually increased.
b. The volume of shale gas loss of core 1427, core 588, core 1146, and core 1162 tested by the shale gas loss simulation experiment in shale were: 1.56, 1.34, 1.79, and 2.01 ml/g, respectively, indicating that the volume of shale gas loss in the Longmaxi group is greater than that in the Niutitang group.

Comparison With the Existing Methods

The existing methods contain the improved USBM method and the curve fitting method. The improved USBM method and the curve fitting method are often used for estimating the volume of shale gas loss and is commonly used in the shale coring (Wei et al., 2015). Under the same circumstances, the

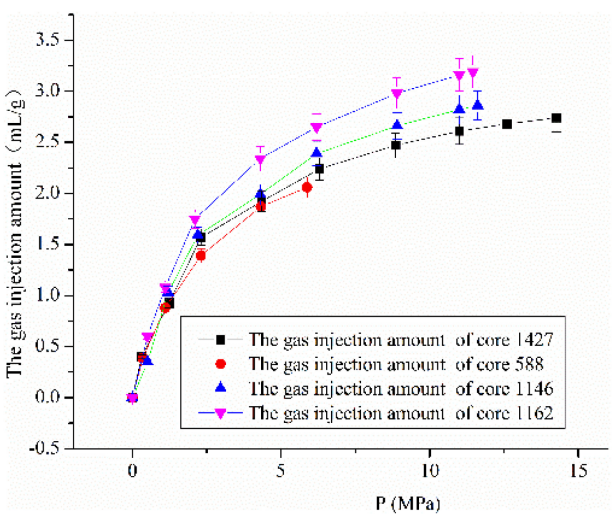

FIGURE 8 | Relationship between the gas injection amount of core and equilibrium pressure.

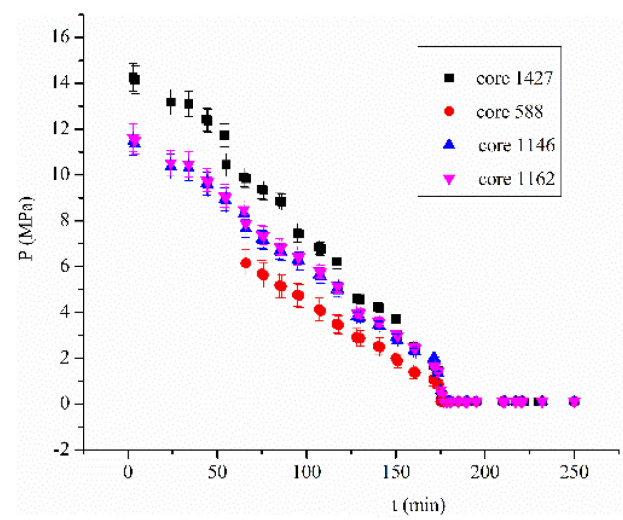

FIGURE 9 | The curve of pressure with time when measuring loss of gas.

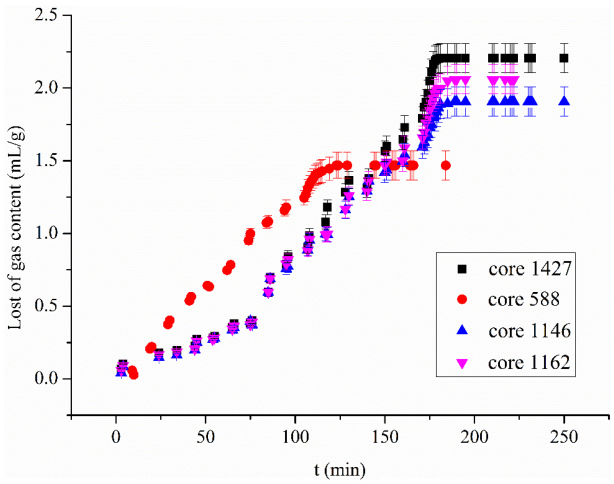

FIGURE 10 | The relationship curve of shale gas loss over time in the experiment.

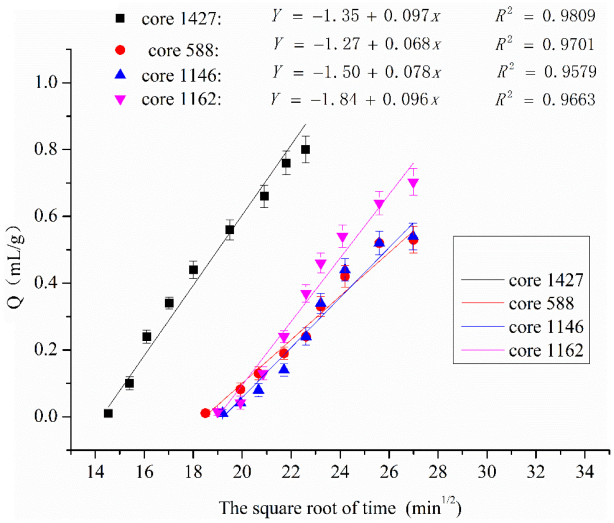

FIGURE 11 | The loss of gas volume in shale obtained by the improved USBM method.

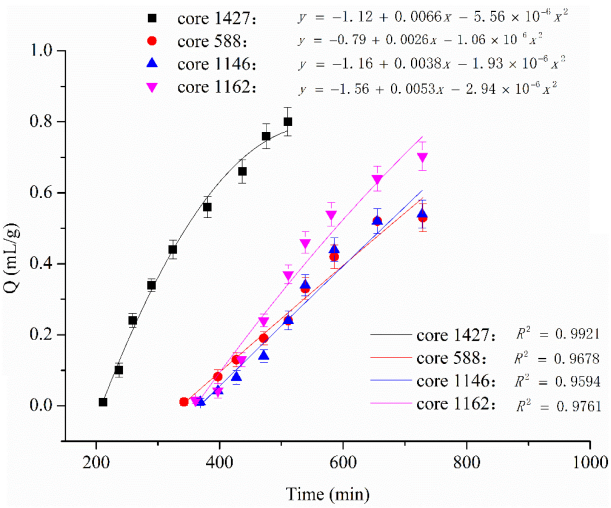

FIGURE 12 | The loss of gas volume in shale obtained by the curve fitting method.

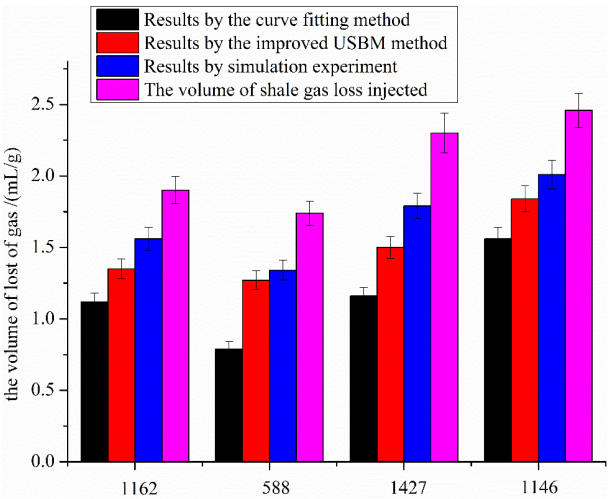

FIGURE 13 | Comparison between the loss of gas obtained by the two methods with the total gas content.

volume of shale gas loss of core 1427, core 588, core 1146, and core 1162 tested by the improved USBM method were: 1.35, 1.27, 1.51, and 1.84 ml/g, respectively. As showed in **Figure 11**. And the volume of shale gas loss obtained by the curve fitting method were 1.12, 0.79, 1.16, and 1.56 ml/g. As showed in **Figure 12**.

The total injection amount of core 1427, core 588, core 1146, and core 1162 were 2.73, 2.29, 2.86, and 3.19 ml/g, respectively in the shale gas loss simulation experiment. And the sum volume of desorbed gas and residual gas (obtained by ball-milling method) were 0.82, 0.55, 0.56, and 0.73 ml/g, respectively. Thus, the volume of shale gas loss of core 1427, core 588, core 1146, and core 1162 injected in the shale gas loss simulation experiment were 1.56, 1.34, 1.79, and 2.01 ml/g, respectively.

We proposed using the error reduction rate of shale loss gas (the percentage of the difference between the volume of shale gas loss obtained by the shale gas loss simulation experiment and the volume obtained by the improved USBM method and curve fitting method and the injected volume in the shale loss gas simulation experiment) to verify the accuracy of the simulation experimental methodology. Conclusion as below:

As showed in **Figure 13** and **Table 5**. Compared with the improved USBM method, the error reduction rates of core 1415, core 1438.5, core 1146, and core 1213 were: 11.05, 4.0, 12.61,

TABLE 5 | Comparison the volume of shale gas loss obtained by three methods.

Sample	The injection amount (ml/g)	Simulation results (ml/g)	Improved USBM method (ml/g)	Error decrease rate (%)	The curve fitting method (ml/g)	Error decrease rate (%)
Core 1427	1.90	1.56	1.35	11.05	1.12	23.16
Core 588	1.74	1.34	1.27	4.00	0.79	31.61
Core 1146	2.30	1.79	1.5	12.61	1.16	27.39
Core 1162	2.46	2.01	1.84	6.91	1.56	18.29

TABLE 6 | Comparison of the characteristics of several typical devices.

Author	Work units	Device characteristics
Kong and Song, 2012	China Coal Geology Bureau First Exploration Bureau	Environment temperature, intermittent reading, decrease of the free gas in the tank, or fill the tank with water
Xu, 2005	Sinopec North China Branch Exploration and Development Research Institute	Helium calibration free space volume, volume flow meter (high speed, sensitive, automatic), temperature rise
Yang et al., 2010	School of Resources and Environment, China University of Mining and Technology	Vacuuming, temperature rise, charge compensation, pressure drop control
Zhang et al., 2011	Xi'an Coal Research Institute	Free space calibration, real-time measurement, vacuuming, temperature rise, injected gas, pressure rise
Requirements for gas loss simulation of experimental rock	Free space calibration, real-time convenient and accurate measurement system, vacuuming, temperature control system (raising the temperature of the specimen to the temperature of the reservoir), charge compensation, pressure drop control	

and 6.91%, respectively. Compared with the curve fitting method, the error reduction rates of core 1415, core 1438.5, core 1146, and core 1213 were 23.16, 31.61, 27.39, and 18.29%, respectively, which proved that the volume of shale gas loss obtained by the simulation experiment was closer to the volume of shale gas loss injected in the simulation experiment. The method of the simulation experiment had higher accuracy.

Discussion

Methodological Analysis

In general, the desorption devices used in the research have advantages and disadvantages. **Table 6** lists several typical methods and their advantages and disadvantages.

Based on the results of sample characterization, the four groups of samples selected in this paper belong to two types of strata with large differences in physical properties. Core 1427 and core 588 belong to the Niutitang Formation, core 1146 and core 1162 belong to the Longmaxi Formation.

In the shale gas loss simulation experiment, the volume of shale gas loss of core 1427, core 588, core 1146, and core 1162 tested by the shale gas loss simulation experiment were: 1.56, 1.34, 1.79, and 2.01 ml/g, respectively, indicating that the volume of shale gas loss in the Longmaxi group is greater than that in the Niutitang group. In the isothermal adsorption test, the max adsorption capacity of core 1427 and core 588 were 2.82 and 2.61 ml/g; The max adsorption capacity of core 1146 and core 1162 were 3.15 and 3.41 ml/g, which demonstrated that the adsorption capacity of the Silurian Longmaxi samples was larger than that of the lower Cambrian Niutitang group. The adsorption/desorption of the Silurian Longmaxi Formation samples with better physical properties is still greater than that of the lower Cambrian Niutitang Formation samples. The results of the isothermal adsorption test, the sample gas injection volume results, and the volume of the shale gas loss reflect that after the microstructure of the sample was destroyed to the same extent, the adsorption and desorption capacity of the Longmaxi sample was still greater than that of the Niutitang group.

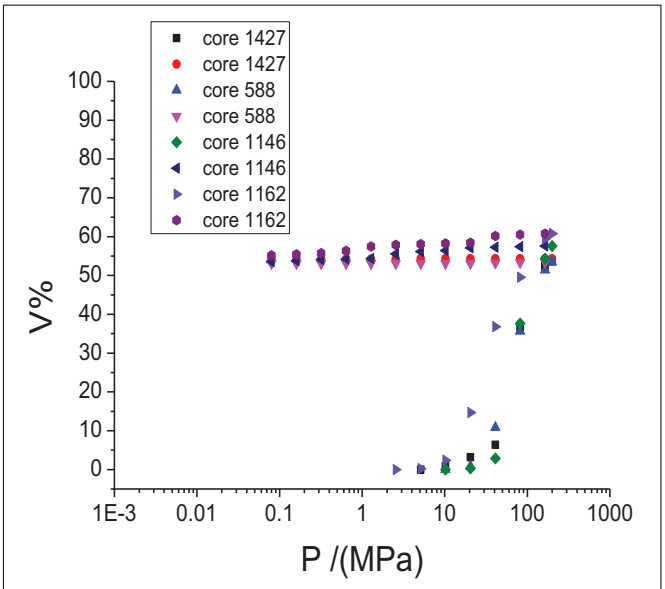

FIGURE 14 | Mercury injection curve.

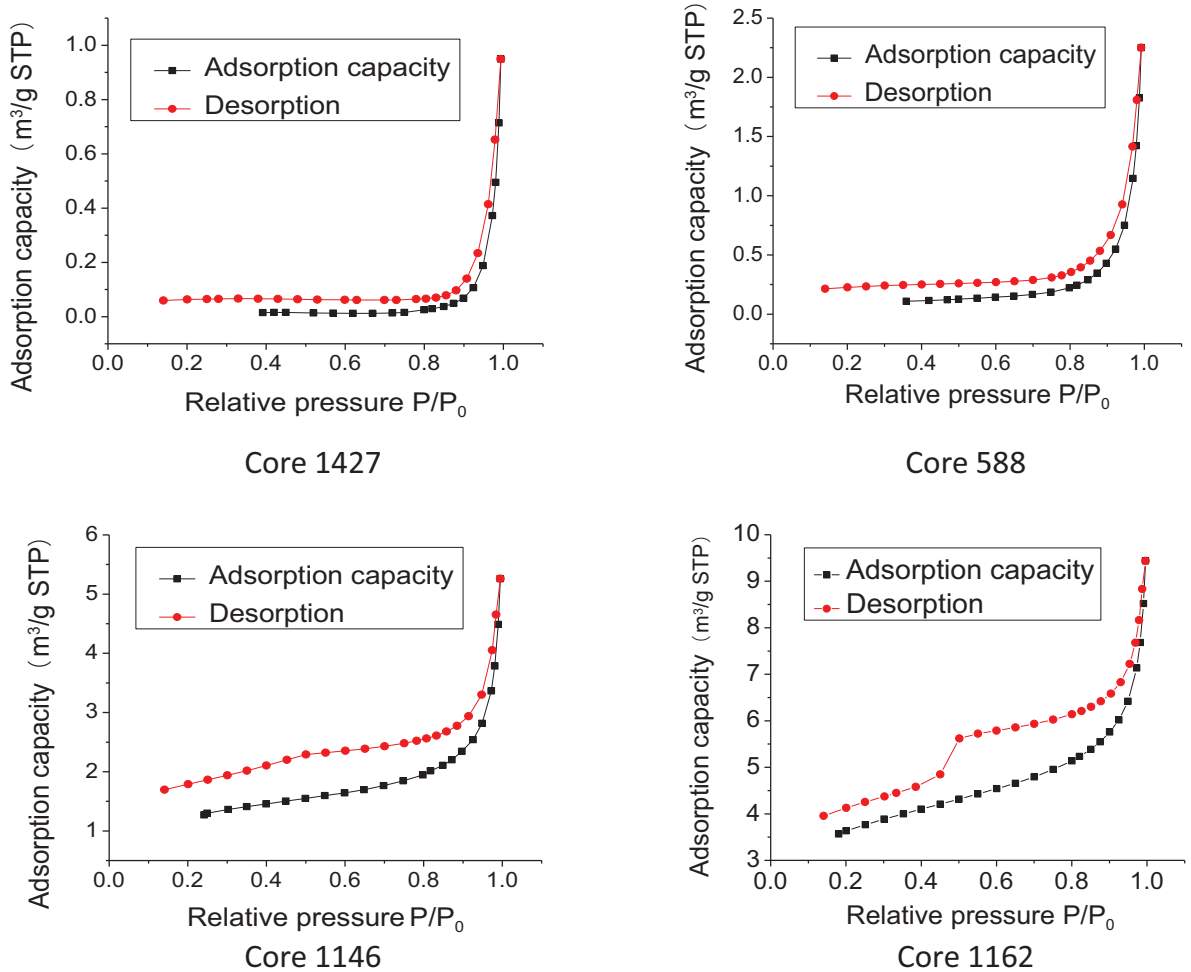

FIGURE 15 | The results by the ASAP2020 system.

Based on the data obtained from the simulation experiment, and comparing the improved USBM method, the curve fitting method, and the simulation experiment method, we infer that:

The amount of shale gas loss obtained by the shale gas loss simulation experiment method is closer to the injected volume of the sample, which indicates that the simulation experiment method is more accurate. Combining the loss time, both the improved USBM method and the curve fitting method use desorption data when the confining pressure drops to 0.1 MPa to invert the volume of shale gas loss. The improved USBM method also requires a linear relationship between the amount of absorption and the square root of desorption time. Combining shale with low gas content, relatively large free gas, and relatively long coring time, the application of the shale gas loss simulation experiment method is wider, and the key lies in whether the sample gas injection can better represent the formation gas content. However, the formation fluid is in dynamic equilibrium, and shale gas loss simulation experiments achieved this through methods such as pressure increase, gas injection, and temperature increase. Especially for fresh samples that have just been corked, it is easier to complete gas injection, and the applicability and accuracy of the shale gas loss simulation experiment method is higher.

Main Controlling Factors

Shale pores

The shape of the high pressure mercury intrusion curve can reflect the developmental characteristics of shale pores. It can be seen from the mercury intrusion-dehydration curve of the four shale samples from the southeastern Sichuan region (**Figure 14**) that the amount of mercury entering the mercury-dehydration curve of each shale sample increased with increasing pressure. The results overall reflect the existence of two types of pore structure in the area of the shale (Hu et al., 2002; Thomas et al., 2013; Liu et al., 2015). In the low pressure part (p < 10 MPa), there is only a small amount of mercury ingress, indicating that pores in this pressure range basically did not develop. When the pressure was between 10 and

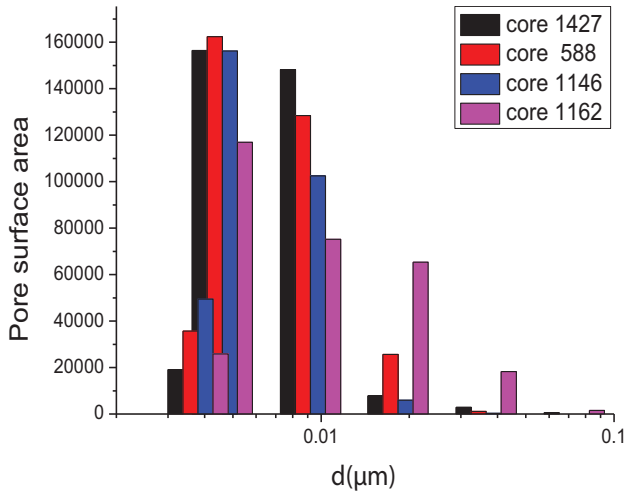

FIGURE 16 | Shale pressure hole distribution curve.

30 MPa, the amount of mercury increased slowly with increasing pressure. This pressure range mainly developed pores larger than 20–50 nm. When the pressure reached about 30 MPa, the amount of mercury entering began to increase rapidly. At pressures greater than 150 MPa, the amount of mercury entering slowed down, and the maximum amount of mercury was still increasing until the maximum pressure was reached, indicating that there was a large number of pores smaller than 10 nm in the shale. According to **Figure 14**, the amount of mercury in the Silurian Longmaxi Formation samples was higher than that in the lower Cambrian Niutitang Formation samples (core1162 > core1146 > core588 > core1427, as shown in **Figure 14**), reflecting that the pores of the Silurian Longmaxi Formation samples were more developed.

Based on the results of the NMR test of the sample, the pore size distribution curves of the shale samples from the Lower Silurian Longmaxi Formation and the lower Cambrian Niutitang Formation sample were compared (**Figure 2**). The position of the main peak of the aperture distribution curve of the Longmaxi Formation is relatively high, indicating that the shale has a relatively large pore size and that the pores are relatively developed. The secondary peaks in the red circle clearly indicate the development of macropores or microcracks (Coates et al., 1999). In addition, there is less distance between the main peak and the secondary peak of the discontinuous range of aperture distribution curves, indicating the development of transition pores and relative uniformity of the shale, which are favorable for connectivity between pores (Liu et al., 2018; Lu et al., 2019). According to the International Union of Pure and Applied Chemistry (IUPAC), pores can be classified as micropores (less than 2 nm), mesopores (2–50 nm), or macropores (greater than 50 nm), depending on their relative sizes (Thommes et al., 2015; Zhou et al., 2018). The pore size distributions of different shales are shown in **Figure 2**. The main peaks of core 1427, core 588, core 1146, and core 1162 were 0.001 μm, 0.02 μm, 0.06 μm, and 0.5 μm, respectively. The macropores and mesopores of the Longmaxi Formation developed mainly from 10 to 250 nm. The large holes in the shale of the Niutitang Formation group are significantly lower, mainly composed of 2–50 nm mesopores.

According to the results of the ASAP2020 test, the maximum adsorption amount of core 1146, core 1162, core 1427, and core 588 were 5.5, 9.5, 1, and 2.4 m^3/g, respectively, indicating that

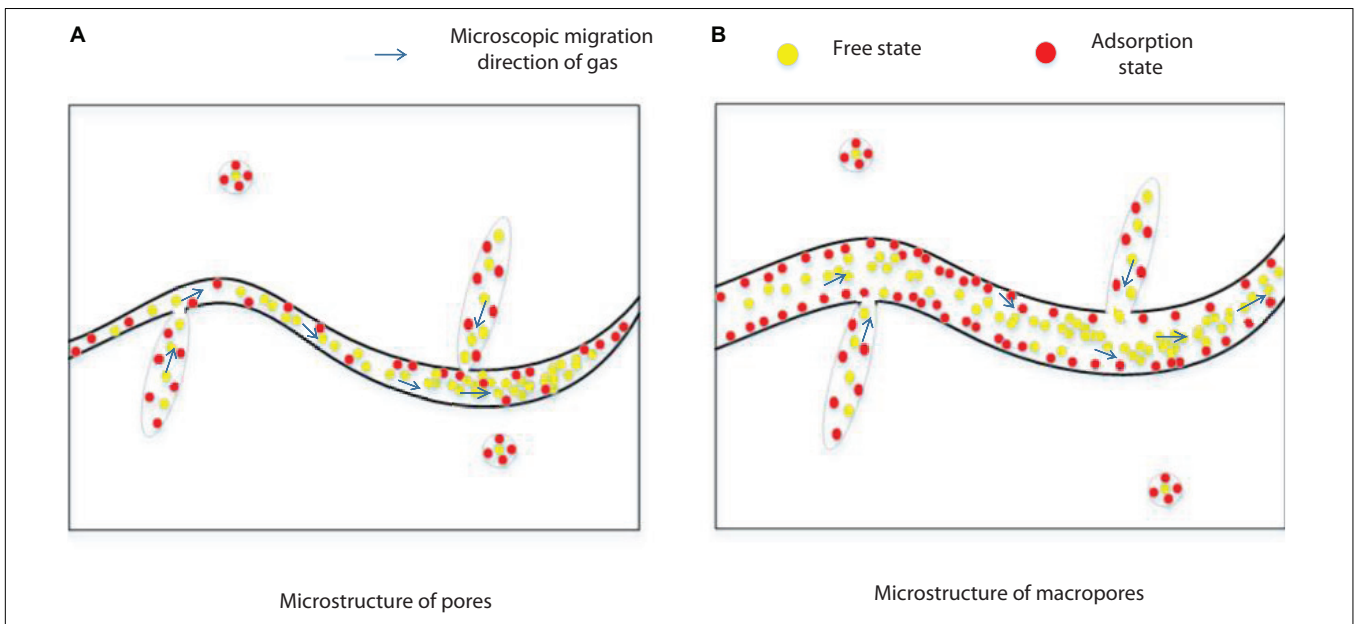

FIGURE 17 | Comparison of the microstructure of large and small pores. **(A)** represents the microscopic pores with poor physical properties, and **(B)** represents the microscopic pores with better physical properties.

the maximum adsorption amount with the relative pressure was reached for core 1162 and core 1146, and the adsorption amounts of core 588 and core 1427 were smaller (**Figure 15**).

BET value of cores

As shown in **Table 6** by the high pressure mercury intrusion method, the BET value of core 1427, core 588, core 1146, and core 1162 were 9.055 m^2/g, 3.1742 m^2/g, 0.0189 m^2/g, and 0.2492 m^2/g, respectively. The pore size distribution is shown in **Figure 16**. The pore surface area of the shale is mainly concentrated at the peaks of the two pore sizes, which are 3–6 nm and 20–50 nm, respectively, and the change rate of the pore surface area with the pore diameter of other pore sizes is almost zero. The pore-contrast surfaces of 3–6 nm and 20–50 nm have a decisive control effect, whereas macropores contribute little to the surface area. Therefore, the BET values of the Silurian Longmaxi Formation samples at 20–50 nm are smaller than those of the lower Cambrian Niutitang Formation samples in the macro hole section (core1162 < core1146 < core588 < core1427), which reflects that the pore seepage resistance of the Silurian Longmaxi Formation samples in the macro hole section is smaller.

TOC and porosity value of cores

As shown in **Tables 1–3**, the quartz content is about 50% in the analysis of the mineral composition of the Niutitang Formation and Longmaxi Formation. The TOC values of core 1427, core 588, core 1146, and core 1162 are 1.63, 2.53, 6.36, and 5.31%. And the TOC values of Longmaxi is higher than that of the Niutitang group. As shown in **Tables 1–3**, the porosity values of core 1427, core 588, core 1146, and core 1162 are 2.89, 2.31, 3.44, and 3.68%.

Overall, the value of pore size distribution, BET, TOC, and porosity reflect that the results of the sample isothermal adsorption test and the shale gas loss simulation experiment results (the adsorption and desorption capacity of the Longmaxi sample is greater than that of the Niutitang sample) (**Figure 17**).

CONCLUSION

In this study, four group shales from the Silurian Longmaxi Formation and the Lower Cambrian Niutang Formation with large differences in physical properties in the eastern Sichuan Basin were selected and shale gas loss simulation experiments were conducted. It proposes using the error reduction rate of shale gas loss (the percentage of the difference between the volume of shale gas loss obtained by the shale gas loss simulation experiment method and the volume obtained by the improved USBM method and curve fitting method and the injected amount of shale gas loss of core) to verify the accuracy of the shale gas loss simulation experiment method. Conclusion as below:

(1) In combination with the actual situation of the shale coring, by means of treating the three stages of the shale well core removal, ground exposure, and water bath heating and desorption as a process of desorption that changes with confining pressure. Measurements such as pressure increase, raising the temperature of the specimen to the temperature of the reservoir, and gas injection were taken for the shale cores extracted from the ground. An indoor shale gas loss simulation experiment method was independently designed to determine the volume of shale gas loss. The method does not need to satisfy the linear relationship between the desorption amount and the square root of the desorption time at the initial stage of desorption. It also does not need to revert back to the desorption amount of hours ago by core desorption data of hours later. Thus, this method has wide application value in the efficient development and utilization of shale gas.

(2) Compared with the improved USBM method, the error reduction rates of core 1415, core 1438.5, core 1146, and core 1162 were: 11.05, 4.0, 12.61, and 6.91%, respectively. Compared with the curve fitting method, the error reduction rates of core 1415, core 1438.5, core 1146, and core 1162 were 23.16, 31.61, 27.39, and 18.29%, respectively, which proved that the shale gas loss simulation experiment method had higher accuracy. In addition, analysis of the main controlling factors shows that the shale pore size distribution, BET value, TOC value, and porosity value have a very important effect on the volume of shale gas loss.

DATA AVAILABILITY STATEMENT

The raw data supporting the conclusions of this article will be made available by the authors, without undue reservation.

AUTHOR CONTRIBUTIONS

JH and JT conceived the idea. JZ and YL conducted the analyses. YL and DJ provided the data. All authors contributed to the writing and revisions.

FUNDING

This work is the partial result of support provided by the Chongqing Science and Technology Commission Project (csts2016zdcy-zd90001), the Natural Science Foundation of Chongqing (cstc2018jcyjAX0542), the Major Research plan of the National Science and Technology in 13th Five-Year Plan (2017ZX05049-003-11), and the Program for Changjiang Scholars and Innovative Research Team in Chongqing University (IRT17R112).

ACKNOWLEDGMENTS

We are very grateful for the project and platform provided by the Chongqing municipal commission of science and technology. We are also very grateful for the careful guidance of tutor Lu Yiyu and teacher Tang Jiren. In the experiment part of this manuscript, we are very grateful for the great assistance from all of you. Finally, we would like to thank the reviewers whose comments improved the quality of the manuscript.

REFERENCES

Ambrose, R., Hartman, C. R., Campos, D. M., Akkutlu, Y., and Sondergeld, C. (2012). Shale gas-in-place calculations part I: new pore-scale considerations. *SPE J.* 17:SE131772.

Coates, G. R., Xiao, L., and Prammer, M. G. (1999). *NMR Logging Principles and Application*. Houston, TX: Halliburton Energy Services. Gulf publishing company.

Dong, Q., Liu, X. P., Li, G. W., and Dong, Q. Y. (2012). Discussion on determination method of shale gas content. *Nat. Gas Oil.* 30, 34–40.

Hao, J., Jiang, Z. X., and Xing, J. Y. (2015). An improved method for estimating gas loss in shale gas. *Geoscience* 29, 1475–1483.

Hu, T., Ma, Z. F., and Yao, H. Q. (2002). Study on isotherm of methane supercritical pressure adsorption. *Nat. Gas Chem. Indus.* 27, 36–41.

Kong, Q. H., and Song, H. Z. (2012). Analysis on testing technology of CBM content and factors influencing test quality. *China CBM* 9, 16–20.

Li, J. Q., Gao, Y. Q., Hua, C. X., and Xia, Z. L. (2014). The experience of shale gas exploration in North America is an inspiration to establish the evaluation system of Marine shale gas in south China. *Petrol. Geol. Recover.* 21, 23–27.

Li, S. L. (2000). *Natural Gas Engineering*. Beijing: Petroleum Industry Press, 84–86.

Liu, H. L., Deng, Z., Liu, D. X., Zhao, Q., Kang, Y. S., and Zhao, H. X. (2010). Method for estimating gas loss in shale gas measurement. *Petrol. Drill. Technol.* 32, 156–158.

Liu, S. X., Zhong, J. H., Ma, Y. S., Yi, C. M., Liu, C. L., Li, Z. X., et al. (2015). Study on microstructure of carboniferous shale and isothermal adsorption of shale gas. *J. China Univ. Petrol. (Nat. Sci. Ed.)* 39, 33–42.

Liu, Y., Yao, Y., Liu, D. M., Zheng, Z. J., Shen, G. X., and Chang, Y. H. (2018). Shale pore size classification: an NMR fluid typing method. *Mar. Petrol. Geol.* 96, 591–601. doi: 10.1016/j.marpetgeo.2018.05.014

Lu, Y. Y., Chen, X. Y., Tang, J. R., Li, H. L., Zhou, L., Han, S. B., et al. (2019). Relationship between pore structure and mechanical properties of shale on supercritical carbon dioxide saturation. *Energy* 172, 270–285. doi: 10.1016/j.energy.2019.01.063

Meng, Z. P., Liu, C. L., and Ji, Y. M. (2013). Geological conditions and comparative analysis of CBM/shale gas development. *J. Coal* 38, 728–736.

Ray, J. A., Robert, C. H., and Mery, D. C. (2010). *New Pore-scale Considerations for Shale Gas-in-Place Calculations*. Richardson, TX: Society of Petroleum Engineering.

Seidle, J. P., and Metcalfe, R. S. (1991). *Development of Coalbeds Methane*. Richardson, TX: Society of Petroleum Engineering.

Shang, Z. J. (2014). Study on calculation of leakage amount by direct determination method of gas content. *Coal Mine Safety* 43, 1–4.

Smith, D. H., and Williams, F. L. (1984). Diffusion models for gas production from coal: determination of diffusion parameters. *Fuel* 63, 256–261. doi: 10.1016/0016-2361(84)90047-4

Span, R., and Wagner, W. A. (1996). new equation of state for carbon dioxide covering the fluid region from the triple-point temperature to 1100 K at pressure up to 800 MPa. *J. Phys. Chem. Ref. Date* 25, 1509–1595. doi: 10.1063/1.555991

Stotsky, J. A., and Bortz, D. M. (2019). A posteriori error analysis of fluid–structure interactions: time dependent error. *Comput. Methods Appl. Mech. Eng.* 356, 1–15. doi: 10.1016/j.cma.2019.07.009

Su, J., Shen, Y. C., Jin, H., Liu, B., and Hao, J. (2017). Shale gas content calculation of the triassic Yan Chang formation in the southeastern ordos basin China. *Energies* 10, 1–18.

Sun, B. J., Zhang, Y. L., Du, Q. J., and Shen, Z. H. (2013). Evaluation of adsorption and desorption performance of CO_2 in shale. *J. China Univ. Petrol.* 37, 95–99.

Tang, J. R., Wang, X. C., Lu, Y. Y., Ao, X., Han, S. (2018). Experimental study on time effect and deformation anisotropy of shale and coal under CO_2. *J. China Coal Soc.* 43, 2288-2295.

Thomas, F. R., Michael, J. B., Andrew, C. A., and Thomas, K. M. (2013). Methane adsorption on shale under simulated geological temperature and pressure conditions. *Energy Fuels* 27, 3099–3109. doi: 10.1021/ef400381v

Thommes, M., Kaneko, K., Neimark, A. V., Olivier, J. P., Rodriguez-Reinoso, F., Rouquerol, J., et al. (2015). Physisorption of gases, with special reference to the evaluation of surface area and pore size distribution (IUPAC Technical Report). *Pure Appl. Chem.* 87, 1051–1069. doi: 10.1515/pac-2014-1117

Tinni, A., Sondergeld, C., and Rai, C. (2018). New perspectives on the effects of gas adsorption on storage and production of natural gas from shale formations. *Petrophysics* 59, 17–21.

Wang, J. J., Yang, Z., Dong, M., Gong, H., Sang, Q., and Li, Y. (2016). Experimental and numerical investigation of dynamic gas adsorption/desorption-diffusion process in shale. *Energy Fuels* 30, 10080–10091. doi: 10.1021/acs.energyfuels.6b01447

Wei, D., Zhang, J. C., Tang, X., Wei, X. L., Li, Z. M., Wang, C. H., et al. (2018). Investigation of gas content of organic-rich shale: a case study from lower permian shale in southern north China Basin, central China. *Geosci. Front.* 9, 559–575. doi: 10.1016/j.gsf.2017.05.009

Wei, Q., Yan, B., and Xiao, X. M. (2015). Progress in the study of shale gas desorption methods. *Nat. Gas Geosci.* 26, 1657–1666.

Xiang, Z. P., Li, Z. J., Chen, C. G., Liu, L. Q., Huang, X. L., Xiao, Q. H., et al. (2016). The shale gas volume method isotherm adsorption experiment gas state equation is preferred. *Nat. Gas Industry* 36, 73–78.

Xu, C. F. (2005). Discussion on determination method of coal seam gas content. *J. He Nan Univ. Technol.* 24, 106–109.

Yang, M. Q., Liu, J., Ren, S. M., Huang, Z. J., Meng, F. Y., Wu, F. et al. (2016). The application of rock gas geyser in shale gas exploration. *China Petr. Expl.* 21, 120–124.

Yang, Z. B., Qin, Y., Wang, Z. F., Geoff, W., and Wu, C. F. (2010). Desorption and diffusion model of coaled methane in coal cores under drilling fluid conditions and calculation of escape amount. *Sci. China* 40, 171–177.

Yao, G. H., Wang, X. Q., Du, H. Y., Yi, W., Guo, M., Xiang, R., et al. (2016). The adaptability of USBM method in the measurement of shale gas content. *J. Petrol.* 37, 802–806.

Yee, D., Seidle, J. P., and Hanson, W. B. (1993). Gas adsorption on coal and measurement of gas content. *AAPG Stud. Geol.* 38, 203–218.

Zhang, Q. (2009). Simulation test and result analysis of CBM loss gas content. *Chinese J. Coal* 34, 1649–1655.

Zhang, W., Guo, M., and Jiang, Z. (2011). Parameters and method for shale gas reservoir evaluation. *Nat. Gas Geosci.* 22, 1093–1099.

Zhou, J. P., Liu, G. J., Jiang, Y. D., Xian, X. F., Liu, Q. L., and Zhang, D. (2016). Supercritical carbon dioxide fracturing in shale and the coupled effects on the permeability of fractured shale: an experiment study. *J. Nat. Gas Sci. Eng.* 36, 369–377. doi: 10.1016/j.jngse.2016.10.005

Zhou, J. P., Shuang, X., Jiang, Y. D., Xian, X., Liu, Q., Lu, Z., et al. (2018). Influence of supercritical CO_2 exposure on CH_4 and CO_2 adsorption behaviors of shale: implications for CO_2 sequestration. *Energy Fuels* 32, 6073–6089. doi: 10.1021/acs.energyfuels.8b00551

Conflict of Interest: DJ was employed by the company CNPC Chuanqing Drilling International Petroleum Engineering Co., Ltd.

The remaining authors declare that the research was conducted in the absence of any commercial or financial relationships that could be construed as a potential conflict of interest.